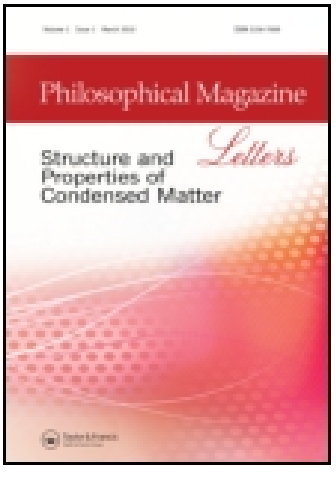

Philosophical Magazine Letters
Publication details, including instructions for authors and subscription information:
http://www.tandfonline.com/loi/tphl20

Formation of omega and Ti_2Ni phases in a residual Ti-Ni-Ti multilayer between stainless steel and zirconia after bonding at 1173 K

Shen-Hung Wei[a] & Chien-Cheng Lin[a]
[a] Department of Materials Science and Engineering, National Chiao Tung University, Hsinchu 300, Taiwan
Published online: 02 Sep 2014.

To cite this article: Shen-Hung Wei & Chien-Cheng Lin (2014) Formation of omega and Ti_2Ni phases in a residual Ti-Ni-Ti multilayer between stainless steel and zirconia after bonding at 1173 K, Philosophical Magazine Letters, 94:10, 609-619, DOI: 10.1080/09500839.2014.951705

To link to this article: http://dx.doi.org/10.1080/09500839.2014.951705

Philosophical Magazine Letters, 2014
Vol. 94, No. 10, 609–619, http://dx.doi.org/10.1080/09500839.2014.951705

Formation of omega and Ti_2Ni phases in a residual Ti–Ni–Ti multilayer between stainless steel and zirconia after bonding at 1173 K

Shen-Hung Wei and Chien-Cheng Lin*

Department of Materials Science and Engineering, National Chiao Tung University, Hsinchu 300, Taiwan

(*Received 9 December 2013; accepted 3 July 2014*)

Stainless steel (316L) and 8 mol pct Y_2O_3-stabilized zirconia (8Y-ZrO_2) were bonded using a Ti–Ni–Ti multilayer at 1173 K (900 °C) for 1 h. Cross-sectional transmission electron microscopy specimens were prepared by an innovative focused ion beam plus lift-out technique. In addition to acicular α-Ti, the dissolution of Fe, Cr, and Ni diffusing outwards from 316L into β-Ti led to the precipitation of the omega (ω) phase with different variants in the residual Ti foil between 316L and Ni. The ω-phase was not found in the residual Ti foil between Ni and 8Y-ZrO_2, while Ti_2Ni precipitates were precipitated in some α-Ti grains owing to the exclusion of Ni from the β-Ti.

Keywords: bonding; omega phase; interfaces; titanium; stainless steels; transmission electron microscopy

1. Introduction

The joining of stainless steel 316L and 8Y-ZrO_2 (8 mol pct Y_2O_3-stabilized ZrO_2) has attracted increasing attention in planar solid oxide fuel cell applications because it provides excellent thermal stability and electrical conductivity at high temperatures [1,2]. The coefficients of thermal expansion of 316L and 8Y-ZrO_2 are very different (19.5×10^{-6}/ °C for 316L and 10.5×10^{-6}/ °C for FSZ) [3,4]. It is therefore necessary to find a specific multilayer, such as a Ti–Ni–Ti trilayer, that is ductile and suitably reactive to both stainless steel 316L and 8Y-ZrO_2 to enhance the bonding strength and reliability. The Ti layers in Ti–Ni–Ti act as reactive materials to promote chemical bonding, while the Ni layer acts as a buffer layer to absorb strain energies arising from the mismatch in the thermal expansion coefficients.

In commercially pure titanium, the low-temperature α-phase is stable up to approximately 890 °C. Increasing the O, Al, and/or N contents increases the α → β transition temperature. Moreover, the addition of these elements has a significant effect on the mechanical properties of Ti (and Ti alloys) [5]. Metastable β-Ti alloys are such Ti alloys in which the martensitic β → α transformation is suppressed by sufficient concentration of β stabilizing elements (e.g. V, Cr, Zr, Mo, and Fe) [6–10]. The metastable β-phase can transform to an athermal ω-phase upon quenching from the β-phase field, or to an

*Corresponding author. Email: chienlin@faculty.nctu.edu.tw

isothermal ω-phase on ageing at a low temperature. Formation of the ω-phase is generally considered undesirable since it can lead to severe embrittlement of the alloys. Banerjee and Mukhopadhyay reported that the ω-phase resulted from a metastable β-phase in the Ti, Zr, and Hf alloys with the required levels of β-stabilizing elements [11]. Furthermore, Williams et al. reported that the addition of Al, O, Sn, or Zr to metastable β-phase titanium alloys (e.g., Ti–V and Ti–Mo alloys) reduced the volume fraction, the upper temperature limit of formation, and the time of stability of the ω-phase [12].

As mentioned above, athermal and isothermal ω-phases are obtained by quenching and ageing, respectively. The latter occurs through a diffusion process, and the former is formed through the lattice collapse mechanism [11]. The formation of the athermal ω-phase can be explained in terms of a typical TTT diagram [13]. The actual time and temperature values not only depend on the cooling rate but also on the typical alloy additions to the titanium alloy.

The ω-phase is formed from the metastable β-phase by collapsing a pair of neighbouring (1 1 1) planes to the intermediate position, leaving the next (1 1 1) plane unaltered, collapsing the next pair, and repeating this process. This process produces a structure of hexagonal symmetry (called the ideal omega) through a complete double-plane collapse, as described by Silcock [14]. Devaraj et al. showed direct evidence of the collapse of neighbouring $(2\ 2\ 2)_\beta$ planes using high-resolution transmission electron microscopy (TEM) [15]. However, the double-plane collapse in some alloys or at the initial stage of this transformation may not be always complete, leading to a trigonal structure (trigonal ω) [16].

Mixed ω- and β-phases induced by the microsegregation of additions of X are often mistaken for a single β-phase in Ti–X alloys. These two phases can be distinguished under direct observation using TEM. In addition, few studies have been conducted on the ω-phase at the joining interface between the metal and the ceramic because it is difficult to prepare cross-sectional TEM specimens by conventional cutting and grinding techniques.

In this study, stainless steel (316L) and zirconia (8Y-ZrO_2) were bonded using a Ti–Ni–Ti multilayer, and the interfacial microstructures between the base materials and the Ti foils were investigated using analytical electron microscopy. It was supposed that the interfacial reactions took place between base materials and interlayers through atomic interdiffusion mechanisms. The elements, such as Fe, Cr, and Ni, diffusing from 316L to Ti foils are considered as β-Ti phase stabilizers, while O evolving from 8Y-ZrO_2 is a α-Ti phase stabilizer. The objective of this study was to explore the effect of atomic interdiffusion on the phase transformation in the two residual Ti foils between stainless steel (or ZrO_2) and Ni. The formation of the ω-phase in the residual Ti foil was elucidated from a crystallographic perspective with the aid of a model.

2. Experimental procedures

Hot-pressed 8 mol pct Y_2O_3 fully stabilized ZrO_2 (8Y-ZrO_2) (2 mm thick, mainly 91.35 ZrO_2 + HfO_2, 8.65 Y_2O_3 in mol pct) and stainless steel 316L sheets (5 mm thick, mainly 60.8 Fe, 19.3 Cr, 14.2 Ni, 1.7 Mo, 2.0 Mn, and 2 Si in at pct) were isothermally joined with a Ti–Ni–Ti multilayer under 0.1 MPa at 1173 K (900 °C) for 1 h in a tube furnace. The Ni foil (100 μm thick and 99.5 pct pure) and the Ti foils (50 μm thick and

99.5 pct pure) were employed as a core layer and as outer layers, respectively. To prevent the sandwiched samples from being oxidized, they were annealed in an Ar-protective atmosphere. The heating and cooling rates were 5 K/min and 3 K/min, respectively.

Cross-sectional SEM samples were cut and ground along the direction perpendicular to the interface, followed by grinding and polishing. Cross-sectional TEM specimens were prepared by an innovative focused ion beam (FIB) plus lift-out technique (Model Nova 200) [17]. The FIB milling was performed with a Ga^+ ion beam at 30 keV. Prior to the FIB milling, a Pt layer (1 μm thick) was deposited by ion beam chemical deposition using $C_9H_{16}Pt$ as the precursor gas. The Pt layer served as a marker and prevented the outer surface of the sample from being directly exposed to the Ga^+ ion beam implantation during subsequent ion milling operations. After rough milling (7–1 nA), polishing (0.5–0.1 nA), and final polishing (50–10 pA), a thin foil (17 × 2 × 0.05 μm) was cut off, and then a micromanipulator was used to transfer the foil from the sample to a TEM grid for subsequent TEM analyses.

Cross-sectional samples prepared as described above were characterized using analytical SEM (scanning electron microscopy, Model JSM 6500F) and TEM (Model JEM 2000 FX), each with an attached energy-dispersive spectroscope (EDS, Model ISIS 300). The Cliff-Lorimer standardless technique was performed on the TEM/EDS, which was equipped with an ultra-thin Be window so that elements lighter than Na, such as C, N, and O, could be detected accurately [18]. The crystal structures of various phases were obtained from the analyses of selected area diffraction patterns (SADPs) using computer-simulation crystallography software.

3. Results and discussion

Figure 1a shows a BEI (backscattered electron image) of a cross-section of the 316L/8Y-ZrO_2 joint with a Ti/Ni/Ti multilayer after bonding at 1173 K (900 °C) for 1 h. Several reaction zones occurred at the stainless steel 316L/Ti, Ti/Ni, and Ti/8Y-ZrO_2 interfaces. Residual Ti and Ni foils were also observed because of incomplete reactions at these interfaces. The two residual Ti foils, which were mainly composed of α-Ti and β-Ti, exhibited very different microstructures, whereas the residual Ni foil was a single phase with Ti in solid solution. As shown in Figure 1b, the residual Ti foil between 316L and Ni consisted of needle-like α-Ti (98.8 ± 0.4 Ti, 0.5 ± 0.1 Fe, 0.4 ± 0.3 Ni, and 0.3 ± 0.1 Cr in at pct) and scattered Ti_2Ni (65.4 ± 1.9 Ti, 28.8 ± 2.1 Ni, 3.2 ± 0.8 Fe, and 2.6 ± 0.6 Cr in at pct) along with retained β-Ti. At the place, where large Ti_2Ni grains were present, the neighbouring area was depleted of Ni, facilitating the formation of the needle-like α-Ti. The retained β-Ti, consisting of 93.4 ± 1.1 Ti, 3.1 ± 0.5 Fe, 1.8 ± 0.7 Cr, and 1.7 ± 0.8 Ni in at pct, was consistent with the fact that the dissolution of Fe, Cr, and Ni gave rise to the stabilization of β-Ti [19,20]. Figure 1c shows that the residual Ti foil between Ni and 8Y-ZrO_2 contained uniformly dispersed Ti_2Ni precipitates (bright) in the α-Ti phase (dark). In addition, β-Ti could undergo a eutectoid transformation of β-Ti → α-Ti + Ti_2Ni (not shown). The precipitation of Ti_2Ni consumed almost all of the Ni diffusing from the β-Ti grains during cooling, leading to the local transformation of β-Ti → α-Ti in the matrix. The retained β-Ti consisted of 87.8 ± 1.9 Ti, 11.3 ± 1.8 Ni, and 0.9 ± 0.3 O in at pct. A sufficient Ni solute content can suppress the phase transformation of β → α-Ti even though O is a strong α stabilizer. It is well

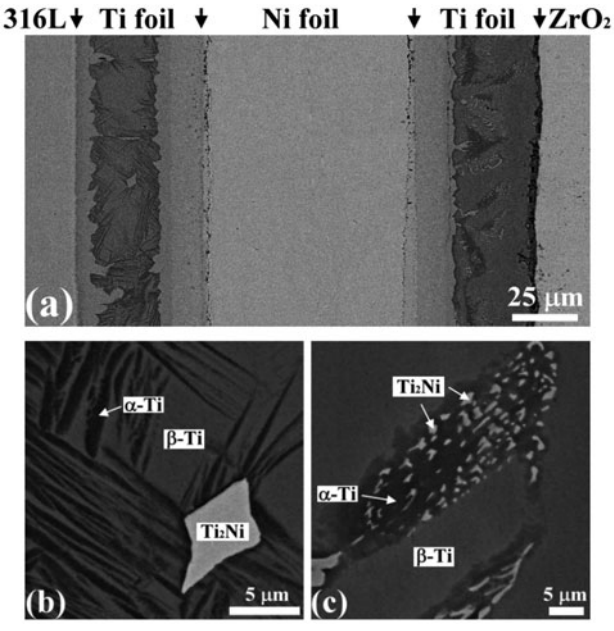

Figure 1. Backscattered electron images of the 316L/8Y-ZrO_2 jointed by a Ti–Ni–Ti trilayer at 1173 K (900 °C) for 1 h: (a) all the reaction layers at a low magnification, (b) residual Ti between the 316L and Ni, and (c) residual Ti between Ni and ZrO_2.

known that ZrO_2 tends to be reduced to oxygen-deficient zirconia (ZrO_{2-x}) in a reducing environment. Because Ti has a high affinity to O, it can act as a reducing agent of ZrO_2. When Ti is in contact with ZrO_2, oxygen can diffuse out of ZrO_2 and be dissolved into Ti, leading to the formation of ZrO_{2-x}. Oxygen ions are readily dissolved and occupy the interstitial sites in Ti up to high concentrations. Some titanium suboxides (e.g. TiO, TiO_2, and Ti_2O_3) are likely formed as the amount of dissolved oxygen increases in Ti. In this study, ZrO_2 was partially reduced by Ti to form ZrO_{2-x}, while oxygen was dissolved into the residual Ti foil to form the intermediate compound TiO (48.2 ± 1.7 Ti, 47.8 ± 2.8 O, and 4.0 ± 1.1 Ni in at pct). No Zr solute was detected in the residual Ti foil between Ni and 8Y-ZrO_2, indicating that the TiO sublayer at the Ti/8Y-ZrO_2 interface could retard Zr diffusion from ZrO_2 into the residual Ti foil.

Figure 2a displays a bright-field image (BFI) of the needle-like α-Ti in the β-Ti matrix within the residual Ti foil between 316L and Ni after bonding at 1173 K (900 °C) for 1 h. At a higher magnification, Figure 2b shows various fine precipitates of the ω-phase in the β-Ti matrix. The diffusion of Fe, Cr, and Ni from the steel resulted in a composition shift in the Ti foil to a metastable β-Ti region. It was such a composition that made the formation of the ω-phase possible [21]. These nanometric ω precipitates (approximately 30 nm) with two different variants (designated as ω_1 and ω_2, respectively) were orientated with a true angle of approximately 109.5°. Silcock reported that there are four crystallographic orientations of the ω-phase with respect to the β-phase [14]. However, only two orientations can be observed along the $[1\,\bar{1}\,0]_{\beta\text{-Ti}}$ zone axis, and the remaining two can be visible in TEM with the incident electron

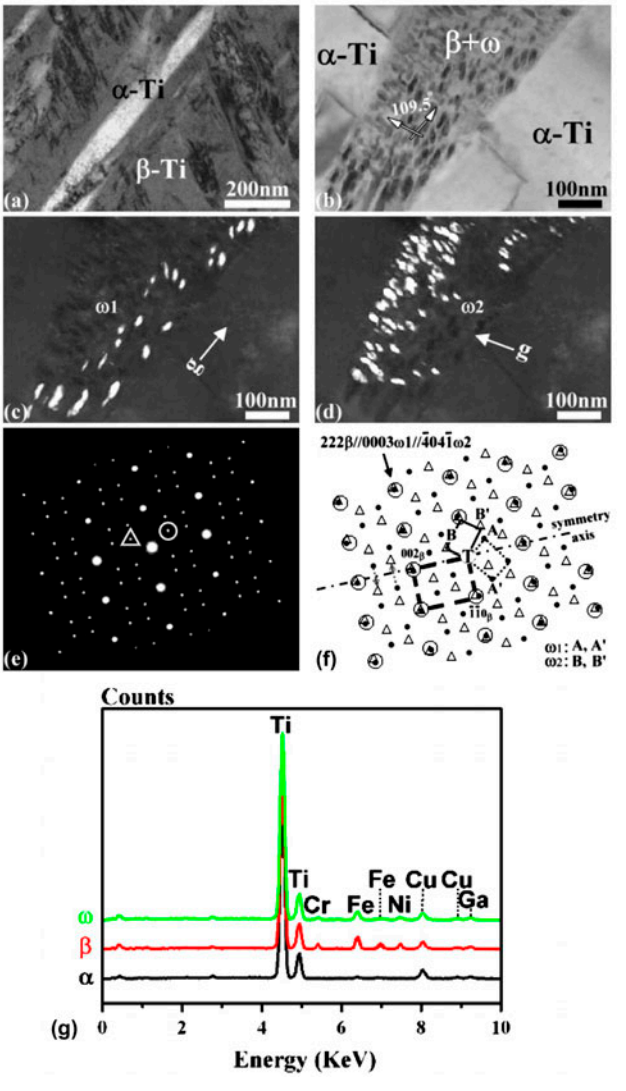

Figure 2. (a) A BFI showing the needle-like α in the β-matrix in the residual Ti foil between the 316L and the Ni after bonding at 1173 K (900 °C) for 1 h, (b) a BFI of the β + ω two-phase structure, (c) and (d) CDFIs showing the different variants of ω precipitates using the $(1\,0\,\bar{1}\,0)_{\omega 1}$ and $(\bar{1}\,0\,1\,0)_{\omega 2}$ diffraction spots, respectively, (e) and (f) SADPs of the β-Ti and ω-phase and their schematic diagrams (O, β-Ti; ●, ω_1; Δ, ω_2) with zone axes of $[1\,\bar{1}\,0]_{\beta\text{-Ti}}$ // $[1\,\bar{2}\,1\,0]_{\omega}$(A: $(1\,0\,\bar{1}\,0)_{\omega_1}$, A′: $(0\,0\,0\,\bar{1})_{\omega_1}$; B: $(\bar{1}\,0\,1\,0)_{\omega_2}$, B′: $(0\,0\,0\,\bar{1})_{\omega_2}$), and (g) the EDS spectra of α-, β-, and ω phases.

beam along the $[1\,1\,0]_{\beta\text{-Ti}}$ zone axis. In this study, the samples were cooled at a moderate rate (about 3 K/min) in furnace, leading to the simultaneous transformations of β → β + α and β → β + ω so that α, β, and ω coexisted in the residual Ti foil between 316L and Ni. The ω-phase was formed preferentially in the solute (Fe, Cr, etc.)-depleted regions of the β matrix in the Ti alloyed with transition metals [22–24],

indicating that some β-stabilizing elements were expelled from the ω-phase during transformation. In alloys, which contain a sufficient concentration of β-stabilizers to suppress athermal ω-phase formation, the metastable β-phase can be subjected to a spinodal decomposition into a solute-rich β-matrix and a corresponding solute-lean β′-phase [22]. The solute-lean β′-phase is thermodynamically favourable for the formation of the isothermal ω-phase. As shown in Figure 2c, the central dark-field image (CDFI) using the $(1\,0\,\bar{1}\,0)_{\omega 1}$ diffraction spot (g vector) revealed the ω_1 precipitates with their longitudinal direction oriented from the lower left to the upper right. As shown in Figure 2d, another CDFI formed by the $(\bar{1}\,0\,1\,0)_{\omega_2}$ diffraction spot revealed the ω_2 precipitates with their longitudinal direction oriented from the lower right to the upper left. The occurrence of the ω-phase in the residual Ti foil could be mainly attributed to the following two factors. First, the dissolution of sufficient β-stabilizers (Fe, Cr, and Ni) retained the metastable β-Ti and made the ω-phase formation thermodynamically favourable. Second, a moderate cooling rate (3 K/min) created favourable kinetic conditions for the ω-phase formation. Moffat and Larbalestier reported the effect of the cooling rate on the β-phase decomposition in Ti–Nb alloys, indicating that the formation of α″ martensite was favoured by a rapid cooling rate, but a relatively slow cooling rate favoured the formation of the ω-phase [25]. Figure 2e displays the SAD patterns of the β + ω two-phase region. In addition to the strong bcc reflections of β-Ti, weak sharp spots corresponded to ω_1 and ω_2, respectively. Previous studies indicated that the crystalline ω-phase formation was limited to less than a 10 at pct solute (Fe, Cr, and/or Ni) content in β-Ti [26], while a solute content of more than 10 at pct led to retained β-Ti with diffuse ω scattering [26,27]. In this study, approximately 9.6 at pct of Fe, Cr, and Ni was dissolved in β-Ti at high temperatures, resulting in the direct transformation of $\beta \rightarrow \beta + \omega$ during cooling. The SADPs were schematically redrawn in Figure 2f, with the diffraction spots being indexed, indicating that the orientation relations between the bcc β-Ti matrix and the hcp ω-phase were recognized as follows: $z = [1\,\bar{1}\,0]_{\beta\text{-Ti}}$ // $[1\,\bar{2}\,1\,0]_{\omega}$ and $(1\,1\,1)_{\beta\text{-Ti}}$ // $(0\,0\,0\,1)_{\omega}$. It was noted that the ω_1 and ω_2 were precipitated in the $\{1\,1\,1\}_{\beta}$ habit planes (forming an octahedron). When the incident electron beam was parallel to the $[1\,\bar{1}\,0]_{\beta\text{-Ti}}$, the view angle between the two variations of the ω-phase was 109.5 (the intersecting angle between $\overrightarrow{TA}$ and $\overrightarrow{TB}$), corresponding to the dihedral angle of the octahedron. Furthermore, a mirror plane $(0\,0\,\bar{2})_{\beta\text{-Ti}}$ of ω_1 and ω_2 was oriented parallel to the incident electron beam, so that the diffraction spots of ω_1 and ω_2 were symmetric with respect to the reciprocal lattice vector $\vec{r}^{*}\,(0,0,-2)_{\beta\text{-Ti}}$. The rotation of the diffraction pattern of ω_1 about $\vec{r}^{*}\,(0,0,-2)_{\beta\text{-Ti}}$ by 180° corresponded to that of ω_2, and vice versa. Figure 2g displays the EDS spectra of α-, β-, and ω- phases in the residual Ti foil between 316L and Ni after bonding at 1173 K (900 °C) for 1 h. The needle-like α-Ti consisted of 98.3 ± 0.6 Ti, 0.8 ± 0.2 Cr, 0.5 ± 0.2 Fe, and 0.4 ± 0.1 Ni in at pct based on TEM/EDS analyses, indicating that the Fe, Cr, and Ni atoms (i.e., β-stabilizers) were hardly dissolved in α-Ti. In contrast, the β-Ti matrix contained approximately 9.6 at pct β-Ti stabilizers, such as 6.0 ± 1.2 Fe, 1.9 ± 0.6 Cr, and 1.7 ± 0.5 Ni in at pct so that the β-Ti was retained at room temperature. The fine precipitates of the ω-phase consisted of 94.3 ± 0.8 Ti, 3.3 ± 0.6 Fe, 1.3 ± 0.4 Ni, and 1.1 ± 0.2 Cr in at pct within the residual Ti foil between 316L and Ni. Artefacts of additional Cu and Ga signals were induced by the copper grid and FIB operation, respectively, so that Cu and Ga were excluded from the quantitative analyses for a better comparison between the TEM/EDS and SEM/EDS results.

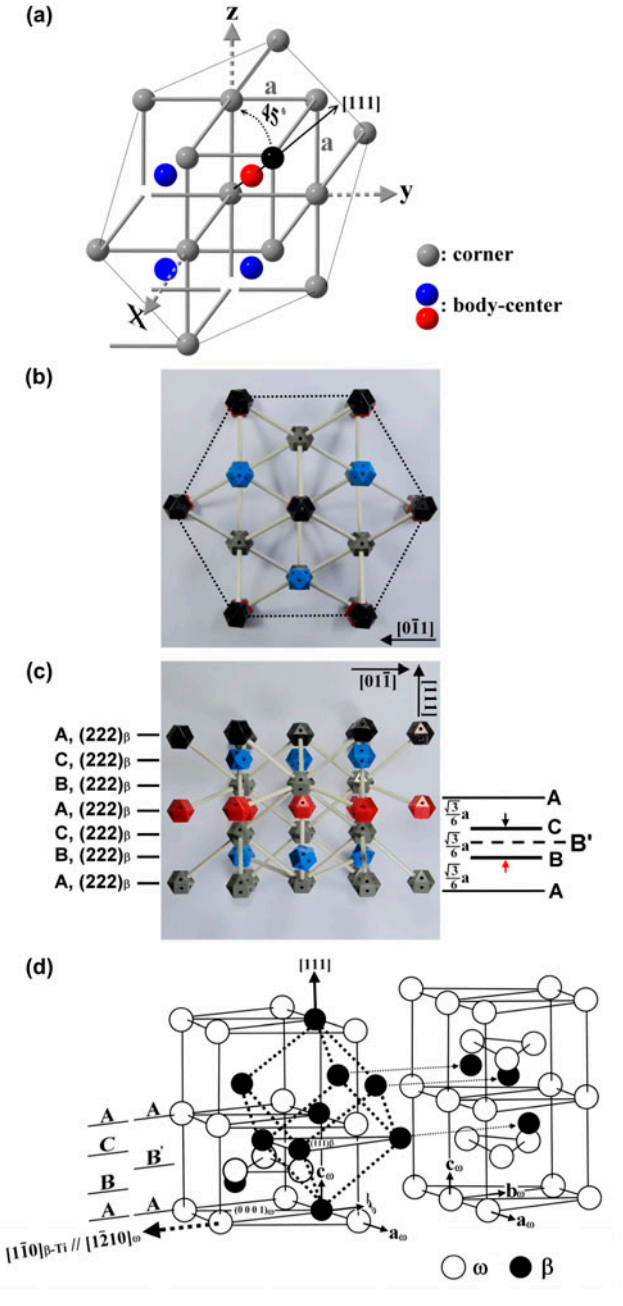

Figure 3. Formation of the crystalline ω-phase from a bcc β-Ti lattice: (a) the bcc β-Ti, (b) the (1 1 1) projection of β-Ti, (c) a side view of the crystal structure in (b), showing the ABCABC sequence of the $(2\,2\,2)_{\beta}$ planes, and (d) the crystallographic relation of the ω-phase and the bcc β-Ti. For clarity, both crystal structures are overlapped and cut away, where $a_{\omega} = [1\,0\,\bar{1}]_{\beta\text{-Ti}}$, $b_{\omega} = [\bar{1}\,1\,0]_{\beta\text{-Ti}}$, and $c_{\omega} = 1/2[1\,1\,1]_{\beta\text{-Ti}}$. The dashed arrows indicate the same atoms in the two cutaway halves.

The formation mechanism of the ω-phase could be described from the crystallographic viewpoint in correlation with the SADPs. Figure 3a shows the bcc unit cell of β-Ti with an atom at each corner (depicted by grey spheres) and an atom at its body centre (depicted by red and blue spheres at various layers). Figure 3b shows the $(1\,1\,1)$ projection of the β-Ti crystal structure, displaying the most closely packed planes in sequence with the black atoms located at the topmost layer. Figure 3c illustrates the β-Ti crystal structure in the edge-on view of $(1\,1\,1)_{\beta}$ along the $[2\,\bar{1}\,\bar{1}]_{\beta\text{-Ti}}$ direction with seven layers, indicating an ABCABC… stacking sequence of $\{2\,2\,2\}_{\beta\text{-Ti}}$. The diffraction spot of $(2\,2\,2)_{\beta}$ was located at the triple distance of the diffraction spot $(0\,0\,0\,1)_{\omega 1}$ away from the direct spot, as shown in Figure 2e, because the distances of A to B, B to C, and C to A were equal to $\sqrt{3}a/6$. Furthermore, Figure 3d shows the crystallographic relationship of the hcp ω-phase (solid line) and the bcc β-Ti (dashed line) with a cut-away view for clarity. While the stacking sequence of β-Ti (solid circles) was ABCABC, the crystal structure of the ω-phase was based on a stacking sequence of AB′AB′ (hollow circles), where B′ was a collapsing pair of $(2\ 2\ 2)_{\beta\text{-Ti}}$ planes. As a result, the orientation relations between the ω-phase (solid line) and β-Ti (dash line) were $(1\,1\,1)_{\beta\text{-Ti}}//(0\,0\,0\,1)_{\omega}$ and $[1\,\bar{1}\,0]_{\beta\text{-Ti}}$ // $[1\,\bar{2}\,1\,0]_{\omega}$, as indicated by the SADPs in Figure 2e.

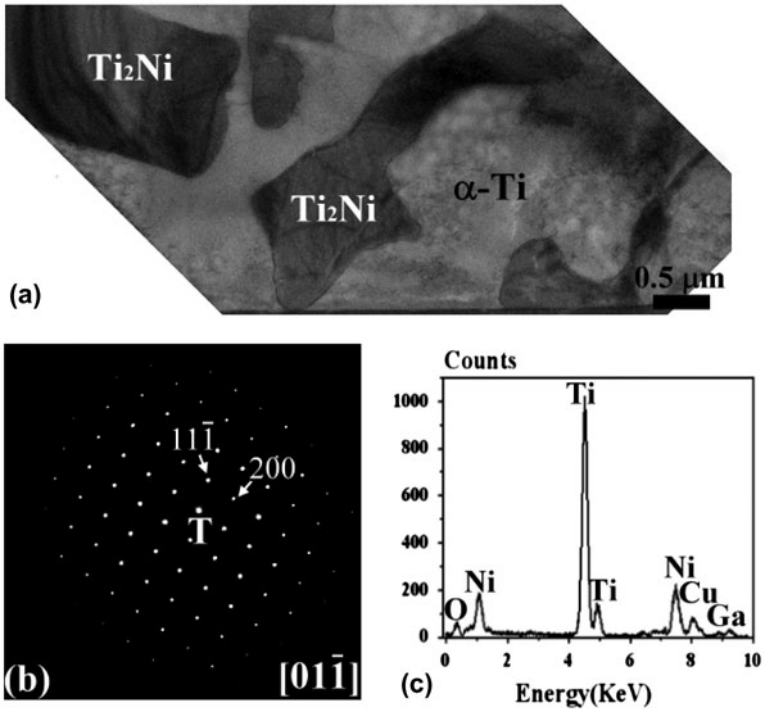

Figure 4. (a) A bright-field image showing the coexistence of α-Ti and Ti_2Ni in the residual Ti foil between Ni and 8Y-ZrO_2 after bonding at 1173 K (900 °C) for 1 h, (b) the SADP of Ti_2Ni with $z = [0\,1\,\bar{1}]$, and (c) the EDS of Ti_2Ni.

Figure 4a displays the BFI of α-Ti and Ti_2Ni in the residual Ti foil between Ni and 8Y-ZrO_2 after bonding at 1173 K (900 °C) for 1 h. Figure 4b shows an SADP of the Ti_2Ni phase along the $[0\,1\,\bar{1}]$ zone axis, corresponding to an fcc structure with a lattice constant a = 1.17 nm (Ti_2Ni, a = 1.131 nm in JCPDS # 720442). Figure 4c shows the EDS of the Ti_2 Ni phase, indicating that the composition of the Ti_2Ni was 65.1 ± 3.7 Ti, 33.2 ± 3.7 Ni, and 1.7 ± 0.4 O in at pct. Additionally, the composition of the α-Ti was 93.9 ± 0.8 Ti, 4.7 ± 0.8 O, and 1.4 ± 0.2 Ni in at pct, indicating that the precipitation of Ti_2Ni led to the Ni depletion in Ti during cooling to room temperature. Artefacts of the Cu and Ga peaks were caused by the copper ring and FIB, respectively, as mentioned above. No ω-phase was found in the residual Ti foil between Ni and 8Y-ZrO_2 because a significant amount of oxygen diffusing out of 8Y-ZrO_2 was dissolved in this residual Ti foil [12].

The identified phases and their EDS results in the two residual Ti foils are summarized in Table 1. The compositions of α, β, ω, and Ti_2N were measured at several different points because a concentration gradient had formed along the direction perpendicular to the interface. Table 1 shows the mean compositions and standard deviations of these phases. The residual Ti foil abutting 316L consisted of α, β, ω, and Ti_2Ni, while the other Ti foil lacked the ω-phase. It is well known that the bonding between base materials and interlayers results from interdiffusion across various interfaces. Consequently, the residual Ti foil neighbouring the 316L contained Fe, Cr, and Ni, and the other Ti foil contained O and Ni. Amongst these elements, Fe, Cr, and Ni

Table 1. Compositions of phases formed at the residual Ti foils after bonding at 1173 K (900 °C) for 1 h.

		Composition (at pct)					
Interlayer	Phase	Ti	Fe	Cr	Ni	O	Notes
Residual Ti between 316L and Ni	α	98.8 ± 0.4	0.5 ± 0.1	0.3 ± 0.1	0.4 ± 0.3	–	SEM/EDS result
	β	93.4 ± 1.1	3.1 ± 0.5	1.8 ± 0.7	1.7 ± 0.8	–	SEM/EDS result
	α	98.3 ± 0.6	0.5 ± 0.2	0.8 ± 0.2	0.4 ± 0.1	–	TEM/EDS result[a]
	β	90.4 ± 1.6	6.0 ± 1.2	1.9 ± 0.6	1.7 ± 0.5	–	TEM/EDS result[a]
	ω	94.3 ± 0.8	3.3 ± 0.6	1.1 ± 0.2	1.3 ± 0.4	–	TEM/EDS result[a]
	Ti_2Ni	65.4 ± 1.9	3.2 ± 0.8	2.6 ± 0.6	28.8 ± 2.1	–	SEM/EDS result
Residual Ti between Ni and 8Y-ZrO_2	α	93.9 ± 0.8	–	–	1.4 ± 0.2	4.7 ± 0.8	TEM/EDS result[a]
	β	87.8 ± 1.9	–	–	11.3 ± 1.8	0.9 ± 0.3	SEM/EDS result
	Ti_2Ni	65.1 ± 3.7	–	–	33.2 ± 3.7	1.7 ± 0.4	TEM/EDS result[a]
	TiO	48.2 ± 1.7	–	–	4.0 ± 1.1	47.8 ± 2.8	SEM/EDS result

[a]Artefact signals for Cu and Ga were removed for a better comparison between TEM and SEM EDS results.

are considered as β-stabilizers, and O is considered an α-stabilizer. The β-phase matrix was found in the residual Ti foil between ZrO_2 and Ni, because it had an extended dissolution of Ni up to 11.3 at pct. Oxygen atoms diffusing from 8Y-ZrO_2 to the residual Ti foil could further retard the formation of the ω-phase and result in the α+β two-phase structure. In contrast, the formation of the ω- and α-phases resulted from the metastable β-Ti with approximately 9.6 at pct of Fe + Cr + Ni in the residual Ti foil between 316L and Ni. Laheurte et al. showed the critical solute concentrations (β_c) of several elements (including Fe, Cr, and Ni) required to retain 100% of the metastable β-Ti on quenching from the β-field [28]. For the metastable β-Ti alloys, the martensitic $\beta \rightarrow \alpha$ is suppressed and an associated ω phase can be formed on quenching and/or ageing. Comparing the α-phases of the two residual Ti foils, one had an insignificant amount of Fe, Cr, and Ni (β-stabilizers), while the other contained a significant amount of dissolved O (α-stabilizer, ~4.7 at pct). It was also noted that the ω-phase contained less β-stabilizers (Fe + Cr + Ni ~ 5.7 at pct) than the β-phase (Fe + Cr + Ni ~ 9.6 at pct) did.

4. Conclusions

The ω-phase was observed in the residual Ti foil in a stainless steel and zirconia joint using Ti/Ni/Ti as an interlayer after annealing at 1173 K/1 h. The diffusion of Fe, Cr, and Ni from the steel to the Ti foils resulted in metastable β-Ti, so that the ω-phase formation might be thermodynamically favourable. It was observed that ω- and β-Ti phases existed along with acicular α-Ti in the residual Ti between the 316L and the Ni, and the metastable-retained β-Ti contained approximately 9.6 at pct β-stabilizers (Fe, Cr, and Ni). Different variants of ω precipitates were observed in the β-matrix. The orientation relationship between the ω-phase and the β-Ti phase was identified as follows: $z = [1\,\bar{1}\,0]_{\beta\text{-Ti}}$ // $[1\,\bar{2}\,1\,0]_{\omega}$ and $(0\,0\,0\,1)_{\omega}//(1\,1\,1)_{\beta\text{-Ti}}$. In contrast, no ω precipitate was found in the other residual Ti foil between Ni and 8Y-ZrO_2 even though the β-Ti (Ni, O) was retained at room temperature. This implied that the solid solution of oxygen could effectively suppress the formation of the ω-phase. The transformation of β-Ti → α-Ti was triggered following the precipitation of Ti_2Ni during cooling. Whether the formation of the ω-phase at the residual interlayer affected the bonding strength should be subjected to further investigation.

Funding

This work was supported by the National Science Council, Taiwan [grant number NSC98-2221-E-009-039-MY2].

References

[1] I. Antepara, I. Villarreal, L.M. Rodríguez-Martínez, N. Lecanda, U. Castro and Laresgoiti: J. Power Sources 151 (2005) p.103.
[2] W.Z. Zhu and S.C. Deevi, Mater. Sci. Eng. A 348 (2003) p.227.
[3] W.B. Hanson, K.I. Ironside and J.A. Fernie, Acta Mater. 48 (2000) p.4673.
[4] I. Yasuda and M. Hishinuma, Electrochemistry 68 (2000) p.526.
[5] G. Lütjering and J.C. Williams, *Titanium*, 2nd ed., Springer-Verlag, Berlin, 2007, p.175.

[6] R. Banerjee, P.C. Collins, D. Bhattacharyya, S. Banerjee and H.L. Fraser, Acta Mater. 51 (2003) p.3277.
[7] W. Sinkler and D.E. Luzzi, Acta Metall. Mater. 42 (1994) p.1249.
[8] B.A. Hatt and J.A. Roberts, Acta Metall. 8 (1960) p.575.
[9] W.F. Ho, J. Med. Biol. Eng. 28 (2007) p.47.
[10] D. De Fontaine, N.E. Paton and J.C. Williams, Acta Metall. 19 (1971) p.1153.
[11] S. Banerjee and P. Mukhopadhyay, *Phase Transformation: Examples from Titanium and Zirconium Alloys*, Pergamon, Oxford, 2007, p.473.
[12] J.C. Williams, B.S. Hickman and D.H. Leslie, Metall. Trans. 2 (1971) p.477.
[13] F.L. Harmon and A.R. Troiano, Am. Soc. Metals 53 (1961) p.43.
[14] J.M. Silcock, Acta Metall. 6 (1958) p.481.
[15] A. Devaraj, S. Nag, R. Srinivasan, R.E.A. Williams, S. Banerjee, R. Banerjee and H.L. Fraser, Acta Mater. 60 (2012) p.596.
[16] R. Pynn, J. Phys. F: Met. Phys. 8 (1978) p.1.
[17] L.A. Giannuzzi and F.A. Stevie, Micron 30 (1999) p.197.
[18] G. Cliff and G.W. Lorimer, J. Microsc. 103 (1975) p.203.
[19] M. Ghosh, K. Bhanumurthy, G.B. Kale, J. Krishnan and S. Chatterjee, J. Nucl. Mater. 322 (2003) p.235.
[20] F.C. Campbell, *ASM Handbook, Elements of Metallurgy and Engineering Alloys*, ASM International, Materials Park, OH, 2008, p.527.
[21] S. Nag, Influence of beta instabilities on the early stages of nucleation and growth of alpha in beta titanium alloys, PhD thesis, The Ohio University, 2008.
[22] Z. Fan and A.P. Miodownik, J. Mater. Sci. 29 (1994) p.6403.
[23] B.S. Hickman, J. Mater. Sci. 4 (1969) p.554.
[24] A.A. Popov, Phys. Met. Metall. 76 (1993) p.524.
[25] D.L. Moffat and D.C. Larbalestier, Metall. Trans. A 19 (1988) p.1687.
[26] W. Sinkler and D.E. Luzzi, Acta. Metall. Mater. 42 (1994) p.1249.
[27] S.L. Sass, J. Less-Common Met. 28 (1972) p.157.
[28] P. Laheurte, A. Eberhardt and M.J. Philippe, Mater. Sci. Eng. A 396 (2005) p.223.